HEARING LOSS

Piplartine attenuates aminoglycoside-induced TRPV1 activity and protects from hearing loss in mice

Marisa Zallocchi[1]*, Sarath Vijayakumar[1], Jonathan Fleegel[1], Lyudmila Batalkina[1], Katyarina E. Brunette[1], Dhaval Shukal[1], Zhiyong Chen[2], Olivier Devuyst[2], Huizhan Liu[1], David Z. Z. He[1], Ali Sajid Imami[3], Abdul-Rizaq Ali Hamoud[3], Robert McCullumsmith[3,4], Martin Conda-Sheridan[5], Luana Janaína De Campos[5], Jian Zuo[1,6]

Hearing loss is a major health concern in our society, affecting more than 400 million people worldwide. Among the causes, aminoglycoside therapy can result in permanent hearing loss in 40% to 60% of patients receiving treatment, and despite these high numbers, no drug for preventing or treating this type of hearing loss has yet been approved by the US Food and Drug Administration. We have previously conducted high-throughput screenings of bioactive compounds, using zebrafish as our discovery platform, and identified piplartine as a potential therapeutic molecule. In the present study, we expanded this work and characterized piplartine's physicochemical and therapeutic properties. We showed that piplartine had a wide therapeutic window and neither induced nephrotoxicity in vivo in zebrafish nor interfered with aminoglycoside antibacterial activity. In addition, a fluorescence-based assay demonstrated that piplartine did not inhibit cytochrome C activity in microsomes. Coadministration of piplartine protected from kanamycin-induced hair cell loss in zebrafish and protected hearing function, outer hair cells, and presynaptic ribbons in a mouse model of kanamycin ototoxicity. Last, we investigated piplartine's mechanism of action by phospho-omics, immunoblotting, immunohistochemistry, and molecular dynamics experiments. We found an up-regulation of AKT1 signaling in the cochleas of mice cotreated with piplartine. Piplartine treatment normalized kanamycin-induced up-regulation of TRPV1 expression and modulated the gating properties of this receptor. Because aminoglycoside entrance to the inner ear is, in part, mediated by TRPV1, these results suggested that by regulating TRPV1 expression, piplartine blocked aminoglycoside's entrance, thereby preventing the long-term deleterious effects of aminoglycoside accumulation in the inner ear compartment.

INTRODUCTION

Statistics from the World Health Organization estimate that nearly 20% of the global population lives with a certain degree of hearing loss, with 430 million people having disabling hearing loss (loss of more than 40 dB) (*1*–*2*). Furthermore, according to the World Health Organization, unaddressed hearing loss costs the global economy US $980 billion annually because of health care sector and educational support costs and a reduction in productivity and quality of life. It is expected that by the year 2050, the number of people with disabling hearing loss worldwide will increase to more than 700 million (*1*). Despite these important social and economic ramifications, the US Food and Drug Administration has only recently approved the first therapy for the treatment of cisplatin ototoxicity in a limited number of pediatric patients with cancer (*3*).

Among the factors that can cause acquired deafness, aminoglycoside (AG) treatment is one of the most common (*2*, *4*). AGs are water-soluble antibiotics that exhibit broad-spectrum antibacterial properties (*4*). They are primarily used against Gram-negative bacterial infections, and because of their poor oral bioavailability, they are given intravenously or locally (as aerosols for pulmonary infections) (*4*–*5*). AGs are frequently used in neonatal intensive care units, with 80% of these babies receiving empirical or prophylactic treatment (*6*–*7*). They are also used to treat a variety of life-threatening infections, including sepsis, tuberculosis-associated infections, urinary tract infections, and pneumonia in patients with cystic fibrosis and immunodeficiency (*7*–*8*).

However, AGs carry the risk of adverse side effects, including reversible nephrotoxicity, irreversible neurotoxicity, and sensorineural hearing loss (*8*–*9*). Despite this, they have remained an irreplaceable therapy because of their effectiveness even with the rise in multidrug-resistant bacterial infections (*10*–*11*). With these considerations, although the value of AGs as an essential therapy is undisputable, their use raises serious safety concerns. Thus, further studies must be conducted to prevent these aforementioned serious complications.

To reduce AG damage to the cochlear cells, various therapeutic strategies have been used, including antioxidants, anti-inflammatory agents, channel blockers, and kinase modulators (*12*–*13*). However, clinical trials have been disappointing, possibly because the protection is not robust and falls off at higher doses of the ototoxic agent. More recent studies have used large-scale drug screenings in cell lines, zebrafish, or mouse cochlear explants to identify otoprotective compounds (*14*–*15*). Those strategies have identified compounds such as quinoxalines and ORC-13661 (which has been awarded investigational new drug status by the US Food and Drug Administration), and some of which have shown better treatment efficacy than many benchmark compounds already in use (*N*-acetylcysteine, D-methionine, and dexamethasone) (*12*–*13*, *16*). Nonetheless, additional drugs and mechanisms of action remain to be further explored so that individual or combinatory treatment can be readily developed for complete protection against AG-induced hearing loss (AGIHL).

[1]Creighton University School of Medicine, Omaha, NE 68178, USA. [2]Institute of Physiology, University of Zürich, Zürich CH-8057, Switzerland. [3]Department of Neurosciences, University of Toledo, Toledo, OH 43614, USA. [4]Neurosciences Institute, ProMedica, Toledo, OH 43614, USA. [5]University of Nebraska Medical Center, Omaha, NE 68198, USA. [6]Ting Therapeutics LLC, La Jolla, CA 92037, USA.
*Corresponding author. Email: marisazallocchi@creighton.edu

We have performed an initial screening of a targeted library of small molecules and identified piplartine (PL) as one of the top candidates for protection against AG-induced ototoxicity in zebrafish (*17*). PL is a plant-derived molecule that has been receiving a great amount of attention because of its anticancer properties. PL can selectively kill cancer cells, but not normal cells, by increasing reactive oxygen species production and can suppress tumor growth and metastasis (*18*–*19*). It is also known for its beneficial effects against diabetes, atherosclerosis, and neurodegenerative disorders (*18*–*21*). In addition, PL can act as an antibiotic adjuvant (*21*). Although its mechanism of action in hair cells (HCs) is unknown, in other systems, PL's activity has been associated with the regulation of various signaling pathways, including phosphatidylinositol 3-kinase/Akt/mammalian target of rapamycin, signal transducer and activator of transcription–3, reticular activating system, and nuclear factor κB (*18*–*23*). On the basis of the many beneficial activities described for PL and the protective effect observed in zebrafish in our preliminary studies, we decided to further investigate its potential for the treatment of hearing loss because of AG ototoxicity.

RESULTS

Characterization of PL's beneficial activity in vitro and in zebrafish

Given our initial experiments showing that PL has the potential to protect zebrafish HCs from neomycin and gentamicin ototoxicity, we decided to assess PL's efficacy against AGs and obtain some of its pharmacochemical and biological properties (Fig. 1). Five to 6 days postfertilization (dpf), zebrafish were exposed to kanamycin in the absence or presence of PL, and neuromast HCs were quantified in these animals (Fig. 1, A to E). PL protected HCs from kanamycin damage, with a median effective concentration (EC_{50}) of 0.125 nM. PL alone at high concentrations (Fig. 1A, #1 to #3) was not toxic to the fish or the neuromasts. A toxicity assay performed in the mouse HC line, HEI-OC1 (*24*), showed that PL can kill 50% of the cells at 25.5 μM, about 200,000-fold higher than its effective dose (Fig. 1F). Because PL shares a common chemical motif with the microtubule destabilizer colchicine (Fig. 1F, red in PL's chemical structure), we incubated HEI-OC1 cells with PL's median lethal dose (LD_{50}) or colchicine as previously described (*25*). PL-treated cells were undistinguishable from control cells (Fig. 1, G and H), but, as expected, colchicine-treated cells showed a disruption of microtubule organization (Fig. 1I). These results suggest that the presence of the colchicine motif in PL does not result in microtubule disruption.

Because AG therapy also results in nephrotoxicity (Fig. 1J) (*26*), we evaluated whether PL could protect renal function. For this purpose, we used the zebrafish line *Tg(lfabp::1/2vdbp-mCherry)* that expresses ½vdbp-mCherry in the liver and releases it into the circulation (*27*). The presence of ½vdbp-mCherry in the fish water can be measured by enzyme-linked immunosorbent assay (ELISA) and used as a proxy for proximal tubule dysfunction (*27*). Animals were incubated with PL (EC_{50} = PL3, $\times 1000EC_{50}$ = PL2, and $\times 50{,}000EC_{50}$ = PL1) with or without kanamycin, and ½vdbp-mCherry was measured in the fish water. The results in Fig. 1J show that whereas kanamycin exposure resulted in proximal tubule dysfunction, the coincubation with PL significantly reduced the amount of ½vdbp-mCherry released into the water (PL1, $P = 0.0307$; PL2 and PL3, $P = 0.0013$ versus kanamycin). On the basis of these results, we concluded that proximal tubule integrity was preserved. PL alone did not have any effect on renal function.

Last, we performed drug-drug interaction (DDI) experiments using a fluorescence-based assay to measure the activity of microsomal CYP450 in the presence of increasing concentrations of PL (0.32 to 1 mM). No significant differences were found between microsomes treated with vehicle [dimethyl sulfoxide (DMSO) or phosphate-buffered saline (PBS)] or PL, which suggests that PL does not inhibit CYP450's activity in vitro (Fig. 1K). Conversely, incubation with ketoconozale (ket), a CYP450 inhibitor, resulted in a significant reduction ($P < 0.01$) in the total fluorescence, confirming the functionality of the assay.

Because PL's protection of the HCs may be the result of mechanotransduction (MET) channel blockage (*14*, *15*), we performed FM1-43 uptake experiments (*28*). The FM1-43 dye can be rapidly incorporated (30 s) into HCs through active MET channels; thus, any compound blocking the channel activity will result in a reduction in the dye uptake (*28*). Zebrafish were exposed to the dye with or without PL at 150 pM, which is a dose around the EC_{50} (fig. S1, C and D), or a 100× dose (fig. S1, E and F). The results (fig. S1G) showed that FM1-43 was incorporated into the HCs even at higher PL doses, confirming that PL's beneficial effect is not because of MET blockage. We also performed a disc diffusion assay to assess the lack of interference with kanamycin's bacterial killing activity (*17*). Figure S1 (H to N) confirmed that kanamycin was able to inhibit bacterial growth even in the presence of PL (fig. S1, J, K, and N). No differences were observed in the mean inhibitory growth area even at higher doses of PL (higher than the EC_{50}, 25 and 100 mM) compared with kanamycin alone, which demonstrates the lack of interaction between the two molecules.

In conclusion, these experiments suggest that PL can protect HCs from AG damage within a wide range of concentrations. We also showed that PL protects renal function, has a good therapeutic index (>200,000), does not interfere with AG's antibacterial activity, and shows no DDI. Moreover, PL's mechanism(s) of action does not involve MET channel blockage. These positive features provide the necessary justification to move PL forward for testing in a more relevant model of AGIHL.

PL protects from AGIHL in mice

On the basis of the previous results, we decided to test PL efficacy in a mouse model of AGIHL. For this purpose, we used the mouse strain B6N(Cg)-Cdh23$^{tm2.1/kjn}$ containing the corrected Cdh23 gene, preventing early-onset age-related hearing loss (*29*). Initial dosing showed that PL was well tolerated when given for 17 consecutive days at concentrations ranging from 10 to 40 mg/kg (maximum solubility in corn oil). Figure S2A showed that there were no differences in body weight between control animals receiving corn oil and animals treated with PL. Given this, we chose the highest dose (40 mg/kg) for our studies.

Previous work demonstrated that PL can cross the blood-brain barrier; mice receiving oral PL showed a peak 15 min after treatment with relatively steady-state concentrations in the brain for at least 8 hours (*22*). Thus, to test whether PL can also reach the inner ear, we injected animals intraperitoneally at 40 mg/kg and processed the inner ears for liquid chromatography with tandem mass spectrometry 2 hours after treatment (fig. S2, B to G). A peak corresponding to PL (mass/charge ratio, 318.13) was observed in the cochlear extracts (fig. S2D). This same peak was observed in the reference run (fig. S2B)

and in extracts from untreated animals spiked with PL (fig. S2C), confirming the peak's identity. Cochlea extracts from animals injected with corn oil were used as the negative control (fig. S2E).

Given that PL was well tolerated and could reach the inner ear compartment, we then evaluated the hearing function [auditory brainstem responses (ABRs) and distortion product otoacoustic emissions (DPOAEs)] of animals receiving kanamycin alone (600 mg/kg, twice a day, subcutaneously for 14 days) or in combination with PL (40 mg/kg once a day, intraperitoneally for 17 days starting 1 day before kanamycin) (fig. S2F). Body weight, recorded every day during the treatment, showed that animals gained weight continuously (fig. S2G).

ABR thresholds were significantly elevated after kanamycin treatment ($P < 0.001$) at all frequencies, from 4 to 64 kHz, whereas the cotreatment with PL resulted in an improvement in hearing function (reduction in threshold elevation) (Fig. 2, A to C). From 4 to 16 kHz, ABR thresholds were back to control values, whereas at frequencies of 22.6 kHz and higher, there was a partial, although substantial, recovery compared with kanamycin-only animals. The threshold shift elevations in the kanamycin-alone group were up to 45 dB compared with vehicle controls. Conversely, threshold shift elevations for the kanamycin + PL group were significantly ($P < 0.01$ and $P < 0.001$) reduced by at least 15 dB when compared with the kanamycin-only group (Fig. 2B). No differences were observed between the PL-only group and the vehicle control or baseline groups, suggesting that PL, per se, does not affect inner ear function.

DPOAE thresholds, a measure of outer HC (OHC) function, were also significantly elevated ($P < 0.001$) at frequencies of 11.3 kHz and higher for animals receiving kanamycin (Fig. 2, D and E). PL treatment significantly reduced kanamycin's effect at 11.3 kHz ($P < 0.0001$) and 16 kHz ($P = 0.0167$) but not at 22.6 kHz ($P = 0.5329$) (Fig. 2E). This latter result was in accordance with the ABR recordings, where there was partial protection by PL at frequencies above 22.6 kHz.

Because systemically administered AGs enter the cochlea mostly through the stria vascularis (SV) (*4*, *30*–*31*), we measured the endocochlear potential of the endolymphatic compartment to assess whether the SV was affected by the presence of AGs. No differences

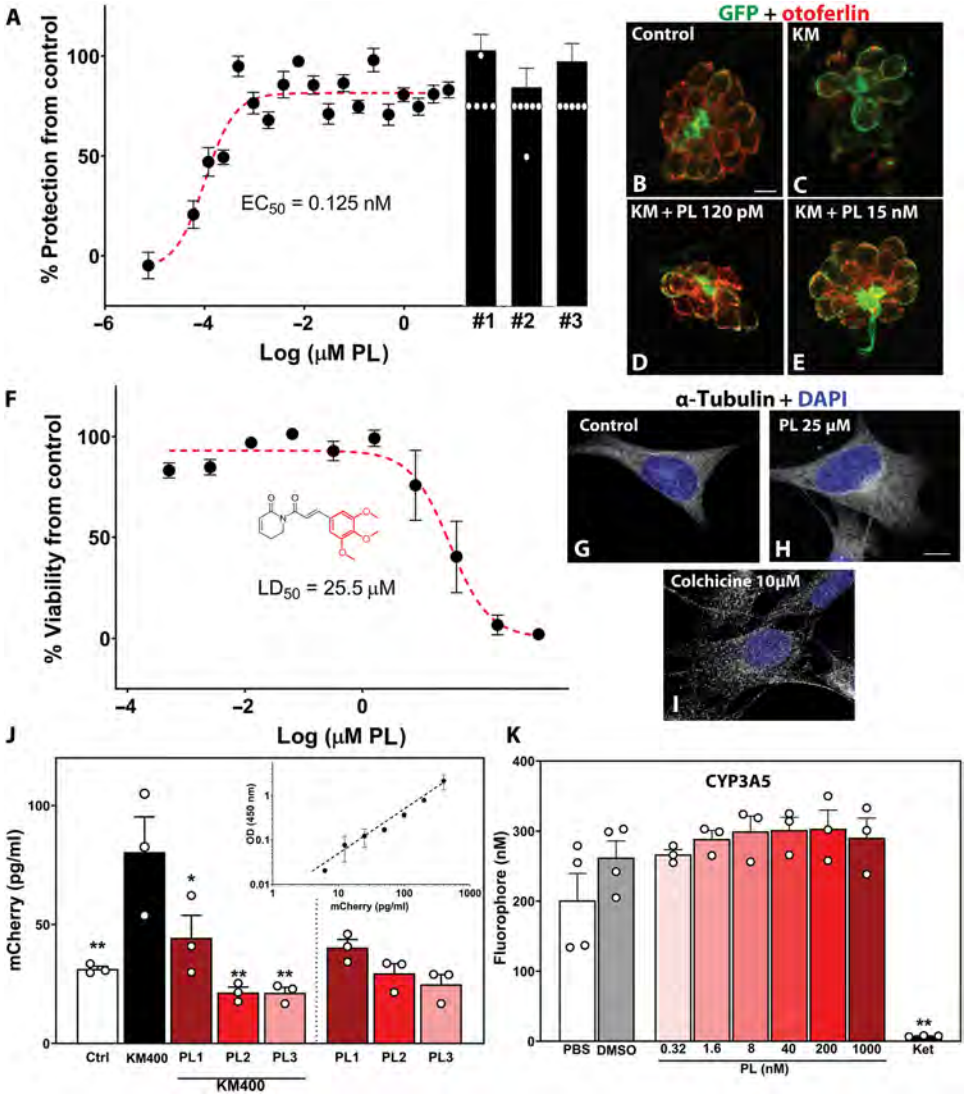

Fig. 1. PL properties. (**A**) Percentage of protection of neuromast HCs. Zebrafish were cotreated with PL (8 µM to 8 pM) and kanamycin (400 µM) and immunostained for otoferlin; 100% represents vehicle-treated fish and 0% kanamycin-treated fish. PL-only: #1 = 25 µM, #2 = 1 µM, and #3 = 0.1 µM. At least three neuromasts per fish were inspected (five or six fish). (**B** to **E**) Representative images of zebrafish green fluorescent protein (GFP)–positive neuromast HCs immunostained for otoferlin (red). Zebrafish were treated with DMSO (control) (B), kanamycin alone at 400 µM (KM) (C), and KM + PL at 120 pM (D) or 15 nM (E). Scale bar, 5 µm. (**F**) Toxicity assay in HEI-OC1 cells. PL, 1 mM to 512 nM. Results are expressed as the percentage of survival from control (three independent experiments). PL's chemical structure is shown with the colchicine motif in red. (**G** to **I**) Representative images of α-tubulin immunostaining (gray) in HEI-OC1 cells from three independent experiments. Vehicle control (DMSO) (G), PL at 25 µM (H), or colchicine at 10 µM (I). Scale bar, 10 µm. (**J**) Proximal tubule function in zebrafish (6 to 7 dpf) measured as in (*26*), in the presence/absence of kanamycin and PL (PL1 = 8 µM, PL2 = 150 nM, and PL3 = 150 pM). Inset indicates the standard curve. Circles represent independent values. OD, optical density. (**K**) Cytochrome activity was assessed by the amount of fluorophore generated in the absence or presence of different PL concentrations. Ket indicates the negative control. Results are presented as the average fluorophore concentration. Means ± SEM. Brown-Forsythe and Welch analysis of variance (ANOVA) followed by Dunnett's T3 posttest for multiple comparisons. *$P < 0.05$ and **$P < 0.01$ versus KM400 (J) or DMSO (K).

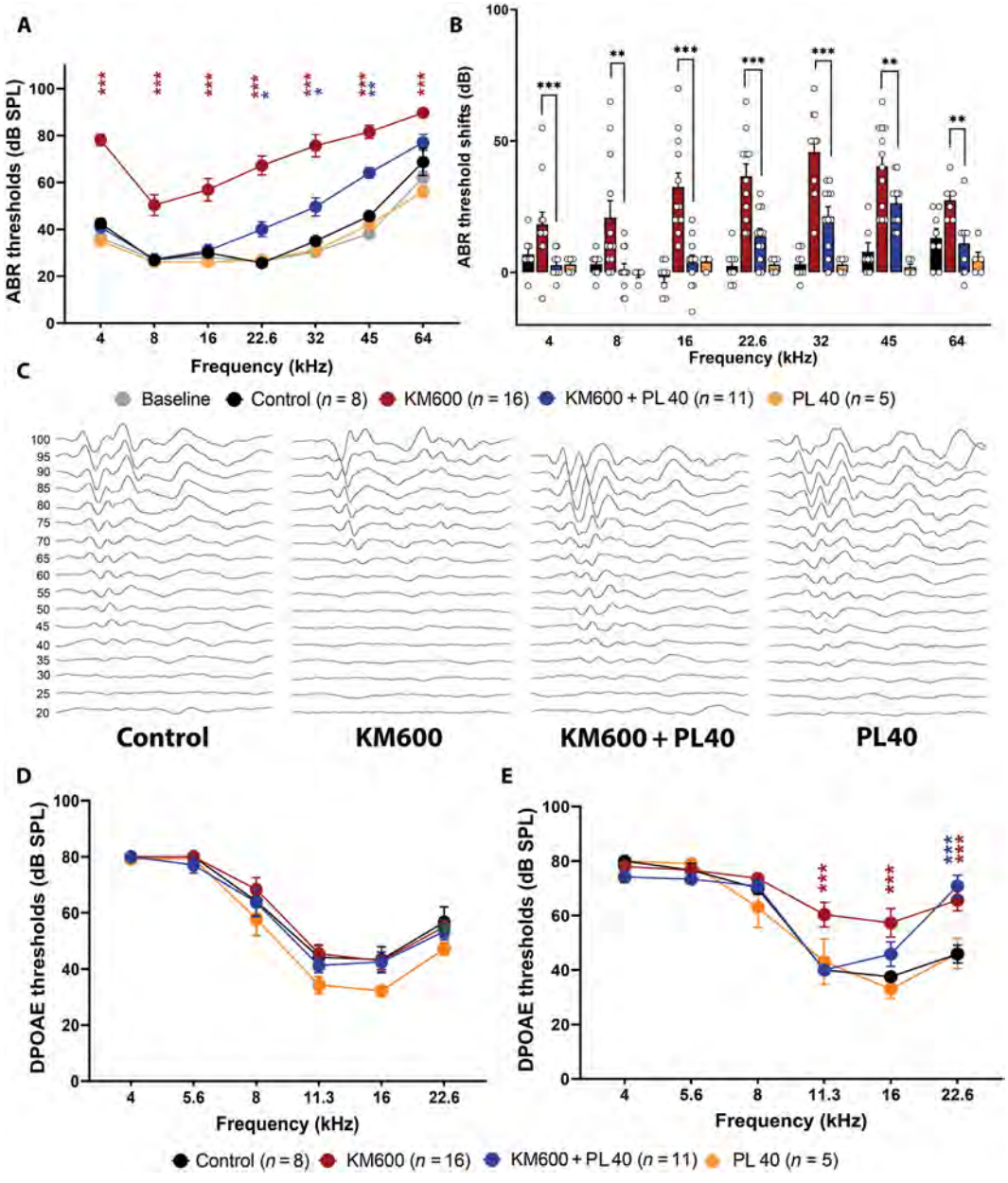

Fig. 2. PL protects from AGIHL in mice. (**A**) ABR thresholds at 4- to 64-kHz frequencies measured before (baseline; gray) and 4 weeks after treatment. Seven- to 8-week-old mice treated with vehicle (black), kanamycin (KM600; red), kanamycin + PL (KM600 + PL; blue), or PL (orange). (**B**) ABR threshold shifts. Means ± SEM. Circles represent individual values. (**C**) Representative ABR traces at the 22.6-kHz frequency for the four treatments. (**D** and **E**) DPOAEs at 4- to 22.6-kHz frequencies measured before (D) and 4 weeks after treatment (E).Threshold averages ± SEM. Two-way [(A), (D), and (E)] and one-way ANOVA (B) followed by Dunnett's posttest for multiple comparisons. *$P < 0.05$, **$P < 0.01$, and ***$P < 0.001$ control versus KM600 [(A), (D), and (E); red], control versus KM600 + PL [(A), (D), and (E); blue], and KM600 versus KM600 + PL (B). Number of animals per group is indicated in parentheses.

were observed among the treatments (fig. S3), suggesting that the chronic administration of AGs does not severely affect SV function and also reinforcing the notion that the sensory epithelium is the main target for AG ototoxicity. These results confirm previous work from Hirose *et al.* (*32*), in which the acute coadministration of kanamycin and furosemide did not produce any significant drop in the endocochlear potential (EP) values ($P = 0.1180$ control versus KM600, and $P = 0.7140$ control versus KM600 + PG40). Overall, the hearing test results suggest that PL can be protective against AG ototoxicity in mammals. No sex differences were observed in terms of body weight gain, treatment and recovery, and degree of PL protection.

PL treatment prevents OHC death and presynaptic ribbon loss

To correlate the hearing tests with inner ear morphology, the organs of Corti from the four groups were stained for the HC marker,

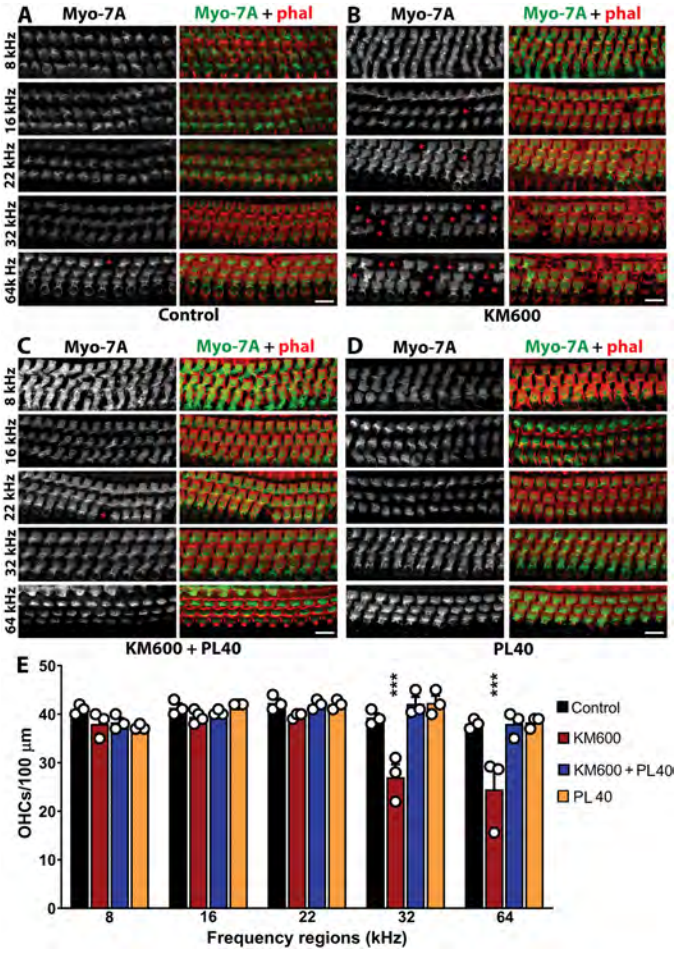

Fig. 3. PL protects OHCs from AG toxicity. (**A** to **D**) Representative micrographs of the organ of Corti at five frequency regions. Control (vehicle) (A), kanamycin (KM600) (B), kanamycin + PL (KM600 + PL40) (C), and PL-only (PL40) (D). Gray scale: myosin-7A (myo-7A) immunostaining alone. Color images: myo-7A (green) and phalloidin (phal) (red). Red asterisks denote missing OHCs. Scale bars, 10 µm. (**E**) OHC quantification (number of animals: control vehicle = 3, KM600 = 3 or 4, KM600 + PL40 = 3, and PL40 = 3) . Means ± SEM. Circles represent individual values. Two-way ANOVA followed by Dunnett's posttest for multiple comparisons. ***$P < 0.001$ versus corresponding control.

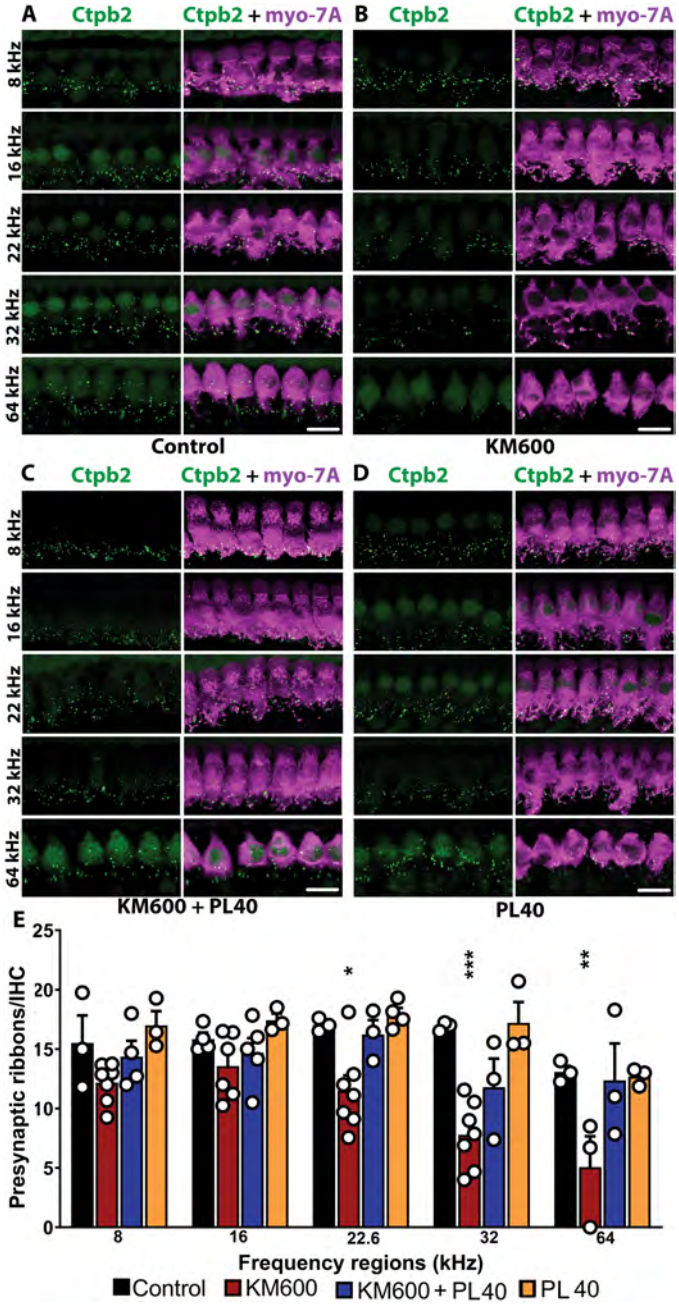

Fig. 4. PL protects presynaptic ribbons from AG-induced toxicity. Representative micrographs of the organ of Corti at five frequency regions. (**A**) Control (vehicle), (**B**) kanamycin (KM600), (**C**) kanamycin + PL (KM600 + PL40), and (**D**) PL-only (PL40). Ctbp2 (green) and myo-7A (magenta) immunostaining. Scale bars, 10 µm. (**E**) Presynaptic ribbon quantification (number of animals: control vehicle = 3, KM600 = 6 or 7, KM600 + PL40 = 3 to 5, and PL40 = 3 or 4). Means ± SEM. Circles represent individual values. Two-way ANOVA followed by Dunnett's posttest for multiple comparisons. ***$P < 0.001$, **$P < 0.01$, and *$P < 0.05$ versus corresponding control.

myosin-7A (Fig. 3, A to D), and the presynaptic ribbon marker, C-terminal binding protein 2 (Ctbp2) (Fig. 4, A to D). The OHCs were imaged and quantified at five frequency regions: 8, 16, 22, 32, and 64 kHz (Fig. 3). Kanamycin treatment resulted in a significant ($P < 0.001$) loss of OHCs at the 32- and 64-kHz regions, whereas PL cotreatment prevented OHC loss (Fig. 3E). At lower frequencies and despite the significant ($P < 0.001$) increase in ABR thresholds because of kanamycin treatment (Fig. 2, D and E), OHCs were still present (Fig. 3E), which suggests that there is additional damage to the sensory epithelium that renders a decrease in auditory function. No deleterious effect was observed in the organ of Corti from animals treated with PL alone.

The quantification of the presynaptic ribbons in the kana-mycin-only–treated group (Fig. 4, A to D) showed a reduction in their number for the 22- to 64-kHz frequency regions (Fig. 4E). Conversely, PL cotreatment resulted in full recovery in their numbers. Similarly to the OHC results, PL alone did not have any toxic effect on the Ctbp2-positive puncta (Fig. 4E).

An increase in ABR thresholds can be the result of a decrease in the number of synaptic contacts between the inner HCs (IHCs) and

the afferent fibers, and this can be reflected in the amplitudes and latencies of the ABR peaks (*33*). Thus, as part of our hearing assessment and because PL treatment did not fully restore inner ear function although OHCs and presynaptic structures were protected, we analyzed wave I amplitudes and latencies (fig. S4).

When analyzing the ABR wave I suprathresholds in the kanamycin-only group, we observed a decrease in wave I amplitudes (fig. S4, A to D) and an increase in latencies (fig. S4, E to H) at all of the tested frequencies (16 to 64 kHz). For the wave I amplitudes at 64 kHz, although the decrease was not significant ($P > 0.05$) (fig. S4D), we still observed a trend in the kanamycin-treated animals. The administration of PL did not fully recover kanamycin's deleterious effect at frequencies between 22.6 and 64 kHz (fig. S4, B to D, G, and H). Compared with vehicle or PL alone, wave I amplitudes were still significantly low ($P < 0.05$), and latencies were significantly delayed ($P < 0.05$) in the kanamycin + PL group. Only at 22.6 kHz did we observe a tendency to counteract kanamycin toxicity, but for frequencies above 22.6 kHz, PL was unable to fully restore inner ear function. These observations correlate with the modest threshold elevation in the ABR recordings after PL cotreatment. The 16-kHz region was used as a positive control because it shows full protection (ABR thresholds similar to controls) after PL cotreatment.

Given the lack of recovery of wave I amplitudes and latencies after PL cotreatment despite the full recovery of the Ctbp2-positive puncta (Fig. 4E), we decided to look at postsynaptic structures. For this purpose, organs of Corti were immunostained for myosin-7A and the neuronal fiber marker, neurofilament H (fig. S5). The intricate network of neuronal fibers innervating the base of the IHCs was analyzed with the Imaris filament tracer tool. No differences were observed among the treatments. Kanamycin alone did not affect the neuronal array: Covered area, volume of the fiber, length, and density were not significantly different ($P > 0.05$) among the four groups (fig. S5E).

In summary, although PL protected OHC and presynaptic ribbons from kanamycin ototoxicity, wave I amplitudes and latencies were not fully reversed. These results suggest that further optimization of PL treatment might be needed.

PL's role in the transient receptor vanilloid 1/AKT1 pathway

To characterize the mechanism(s) through which PL can exert its beneficial effect in the inner ear, we performed a kinome profile analysis of serine/threonine kinases (STKs). The inner ears were microdissected 10 days after receiving the first kanamycin dose, which allowed the emergence of hearing loss (elevation of ABR thresholds; fig. S6) without HC death. The identification of the potential STKs was performed with the PamGene (*34*) kinome platform that contains 144 consensus peptides common to multiple kinases (Fig. 5A). Samples were run in technical triplicates, and the differentially phosphorylated peptides were processed using three different deconvolution strategies (see Materials and Methods and Fig. 5B).

By using this approach, we identified the AKT family members as candidate "hits" contributing to the phosphorylation signal seen across the reporter peptides on the STK chip (Fig. 5C). Immunoblot experiments confirmed the results obtained with the kinome (Fig. 5D). AKT1 phosphorylation (pAKT1) was significantly increased ($P < 0.01$) in the organ of Corti lysates from animals cotreated with kanamycin and PL compared with the rest of the groups. These results are in accordance with previous studies showing the protective effect of AKT activation against neurodegenerative disorders (*35*) and the modulation of AKT's activity by PL (*23*).

Extracellular signal–regulated kinase (ERK) activation was used as a control to reinforce the positive correlation between the kinome results and the immunoblots (Fig. 5E). There was no differential activation of the ERK family members assessed by both approaches, which demonstrates the reliability of the kinome profile.

In addition to the immunoblot studies, we also assessed the expression of pAKT1 in the four groups by immunohistochemistry. Figure 6 (A to L) shows representative images from at least three different animals, with the quantification of the total fluorescence in Fig. 6M. pAKT1 immunostaining was almost negligible in all of the groups except for the kanamycin + PL group. We observed a modest increase in the organ of Corti, at the base of the IHCs, and in the neuronal fibers (Fig. 6, B and M). Strong immunostaining was also observed around the capillaries in the SV and spiral ganglion neurons (SGNs) (Fig. 6, G, K, and M). Overall, the pAKT1 immunohistochemistry results confirmed the kinome and immunoblot analyses and suggest that the regulation of AKT1 may be important for inner ear protection.

During inflammation and AG insult (*36*), cochlear expression of the transient receptor vanilloid 1 (TRPV1) channel is up-regulated in the inner ear, including the SV, SGNs, and HCs (*37*–*38*). This increment in TRPV1 results in an exacerbation of AG ototoxicity because of an increase in AG uptake, with TRPV1 playing a key role during this process (*39*). In addition, TRPV1 activation can affect mitochondrial homeostasis and reactive oxygen species production by preventing AKT activation (*35*). More importantly and directly related to the present work, a recently published study has demonstrated that PL can allosterically antagonize TRPV channel activity (*18*). Given the above information, we assessed TRPV1 expression in the inner ear after treatment (Fig. 7, A to P). As shown before (*32*), chronic administration of kanamycin increased TRPV1 expression in the three compartments (SV, HCs, and SGNs), whereas PL cotreatment resulted in a reduction in TRPV1 expression along the cochlea (Fig. 7Q). PL-only treatment resulted in an increase in TRPV1 expression in supporting cells (inner phalangeal or inner border cells). The quantification of the total fluorescence intensity of the regions of interest from at least three different animals demonstrated the increase in TRPV1 staining because of AG treatment and the reduction during PL therapy (Fig. 7Q). Together, these results suggest that PL's beneficial effect may be mediated, at least in part, by down-regulation and desensitization of TRPV1 and, therefore, a reduction in AG uptake.

Considering the antagonistic effect of PL on TRPV channels described by Conde *et al.* (*18*) and the similarity between TRPV2 and TRPV1 (the closest homologs among the TRPV subfamily) (*39*), we hypothesized that PL may be binding to the same allosteric site in the TRPV1 channel. Therefore, we performed molecular docking and molecular dynamics (MD) simulation experiments to model the interaction between PL and TRPV1's allosteric site (Fig. 8, A to C). First, TRPV1 and TRPV2 were overlaid to extract the putative binding site of PL in TRPV1 using TRPV2 as a guide (fig. S7, A to C). Then, PL was docked into the resulting TRPV1's binding site. Using this information, we analyzed the dynamic behavior of TRPV1 when bound to PL, capsaicin (CP; TRPV1's agonist) (*18*), or the apo receptor (Apo). The results showed that PL bound to TRPV1 leads to conformational changes similar to TRPV2 (*18*) and in

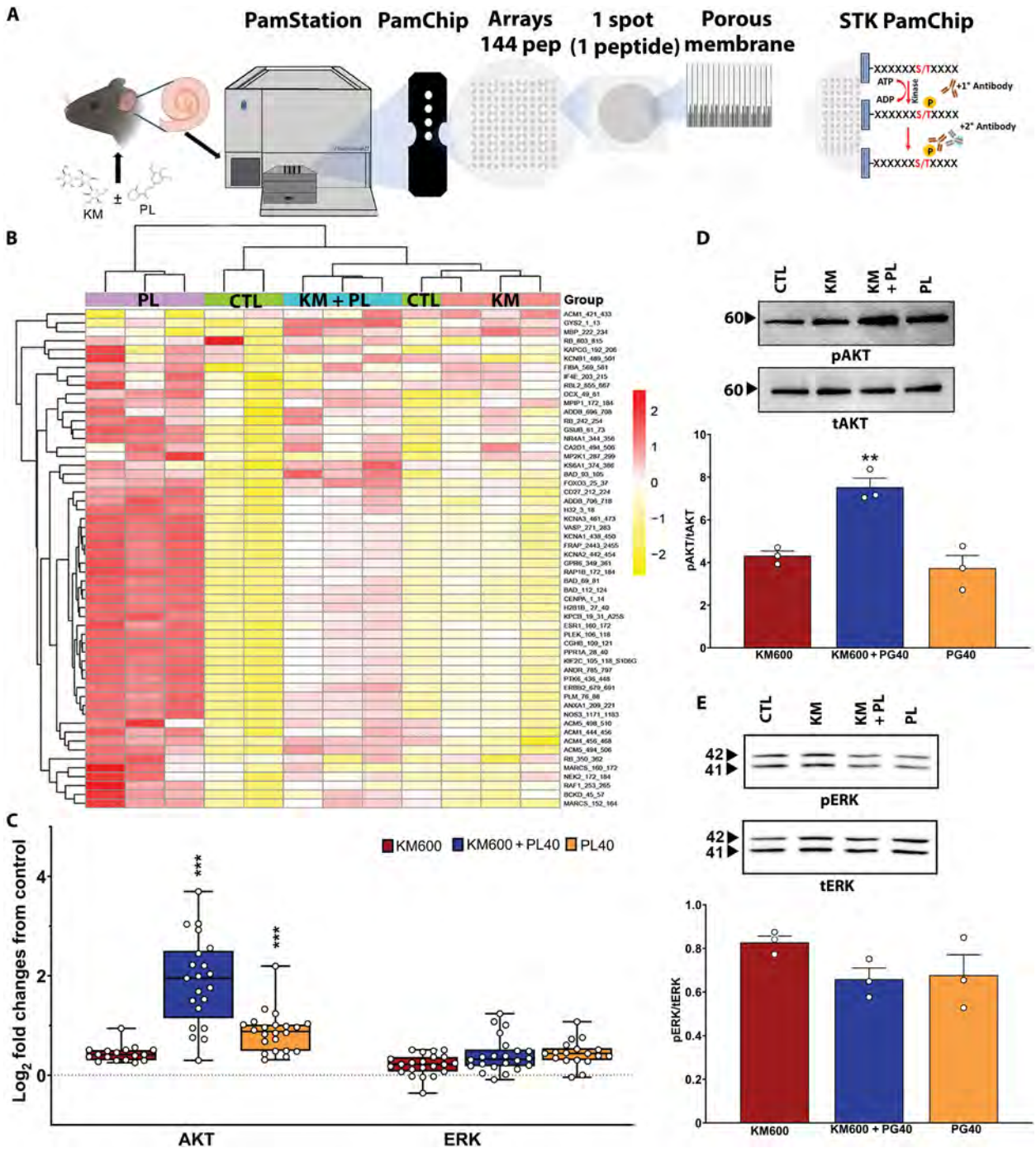

Fig. 5. PL signaling after kanamycin treatment. (**A**) Illustration of PamGene platform workflow. ATP, adenosine 5′-triphosphate; ADP, adenosine 5′-diphosphate. (**B**) Heatmap of phosphorylation activity of the reporter peptides on the STK kinome panel. Unbiased clustering of control (CTL), kanamycin-only (KM), kanamycin + PL (KM + PL), and PL-only (PL). Each row represents a peptide. (**C**) Box and whisker plots of $\log_2$ fold activity changes in reporter peptides "mapped" as putative targets of AKT1 and ERK kinase families (23 and 22 peptides, respectively). An average of triplicates was used for each peptide per condition (four animals were used per treatment condition). (**D**) Top: Representative immunoblots for anti–AKT1-S473 (pAKT). Numbers on the left indicate molecular weights. Bottom: Quantification of at least three independent experiments. Membranes were reprobed with anti-tAKT (total-AKT). (**E**) Top: Representative immunoblots for anti–ERK1/2-T202/Y204 (pERK). Membranes were reprobed with anti-tERK1/2 (total-ERK1/2). Bottom: Immunoblot quantification of at least three independent experiments. Three animals were used per treatment for AKT and ERK immunoblots. Statistical analysis: Two-way ANOVA followed by Dunnett's posttest for multiple comparisons (C) and Brown-Forsythe and Welch ANOVA followed by Dunnett's T3 posttest for multiple comparisons (D). ***$P < 0.001$ and **$P < 0.01$ versus kanamycin.

opposition to the changes induced by CP (Fig. 8, A to C). Overall, PL produces the following structural changes in TRPV1 to maintain the receptor in an inactive (closed) state: The selectivity filter and S6 gate remain closed, and the structure shifts downward relative to the central pore. Similar conformational changes were observed when modeling Apo (Fig. 8, A and B). On the opposite, agonist CP

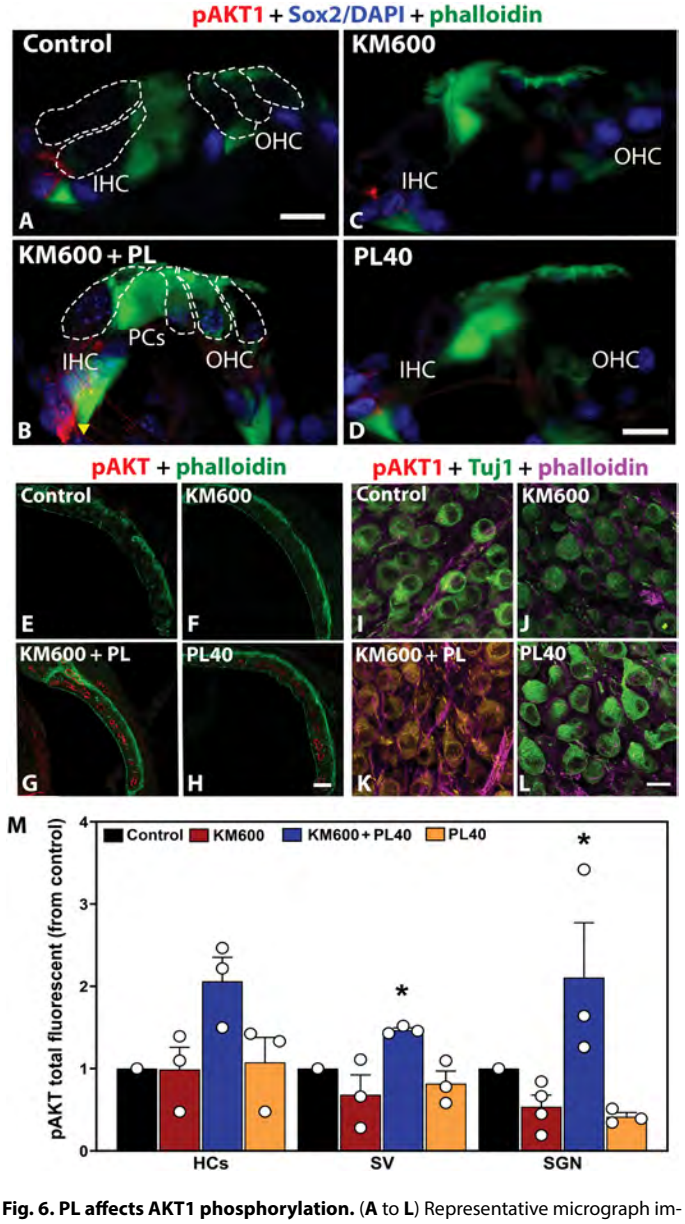

Fig. 6. PL affects AKT1 phosphorylation. (**A** to **L**) Representative micrograph images of cochlea cross sections. [(A) to (D)] Organ of Corti. OHCs and IHCs are delineated with a dashed white line in (A) and (B). PCs, pillar cells. [(E) to (H)] SV. [(I) to (L)] SGNs. Scale bars, 10 μm [(A) to (D) and (I) to (L)] and 20 μm [(E) to (H)]. Samples stained for pAKT1 (red), Sox2/4′,6-diamidino-2-phenylindole (DAPI) (blue), and Tuj1 (I to L) (green). Micrographs were counterstained with phalloidin [(A) to (H), green; (I) to (L), magenta]. (**M**) Quantification is presented as the ratio of fluorescence for each region relative to the total fluorescence. Means ± SEM. Circles represent values from different animals. Three independent samples were analyzed. One-way ANOVA followed by Dunnett's posttest for multiple comparisons. *$P < 0.05$ versus kanamycin.

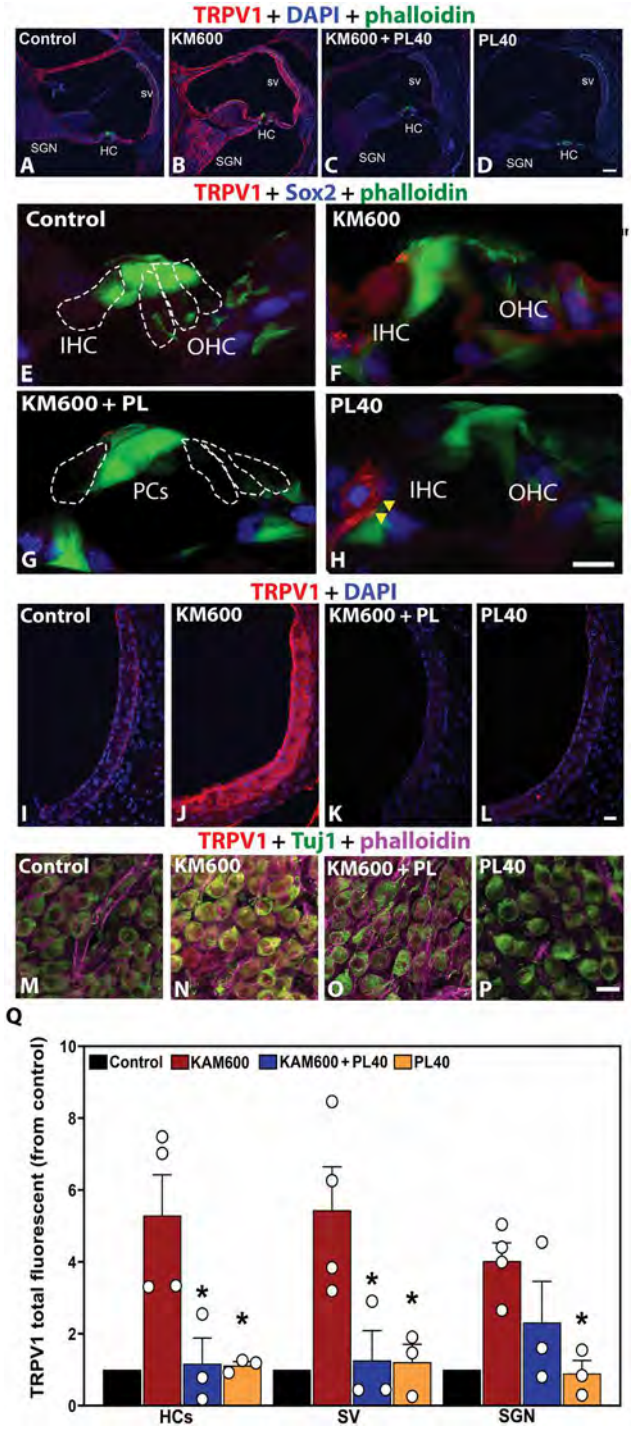

Fig. 7. PL treatment results in TRPV1 down-regulation. (**A** to **P**) Representative micrograph images of cochlea cross sections. (A to D) Low magnification. (E to H) Organ of Corti. OHCs and IHCs are delineated with a dashed white line in (E) and (G). [(I) to (L)] SV. [(M) to (P)] SGNs. Scale bars, 50 μm [(A) to (D)] and 10 μm [(E) to (P)]. Samples were stained for TRPV1 (red), Sox2/DAPI (blue), Tuj1 (green), and phalloidin [green (A) to (H) or magenta (M) to (P)]. (**Q**) Quantification is presented as the percentage of fluorescence for each region of interest relative to the total fluorescence. Means ± SEM. Circles represent values from different animals. Three independent tissue samples were analyzed (three animals per condition). One-way ANOVA followed by Dunnett's posttest for multiple comparisons. *$P < 0.05$ versus kanamycin.

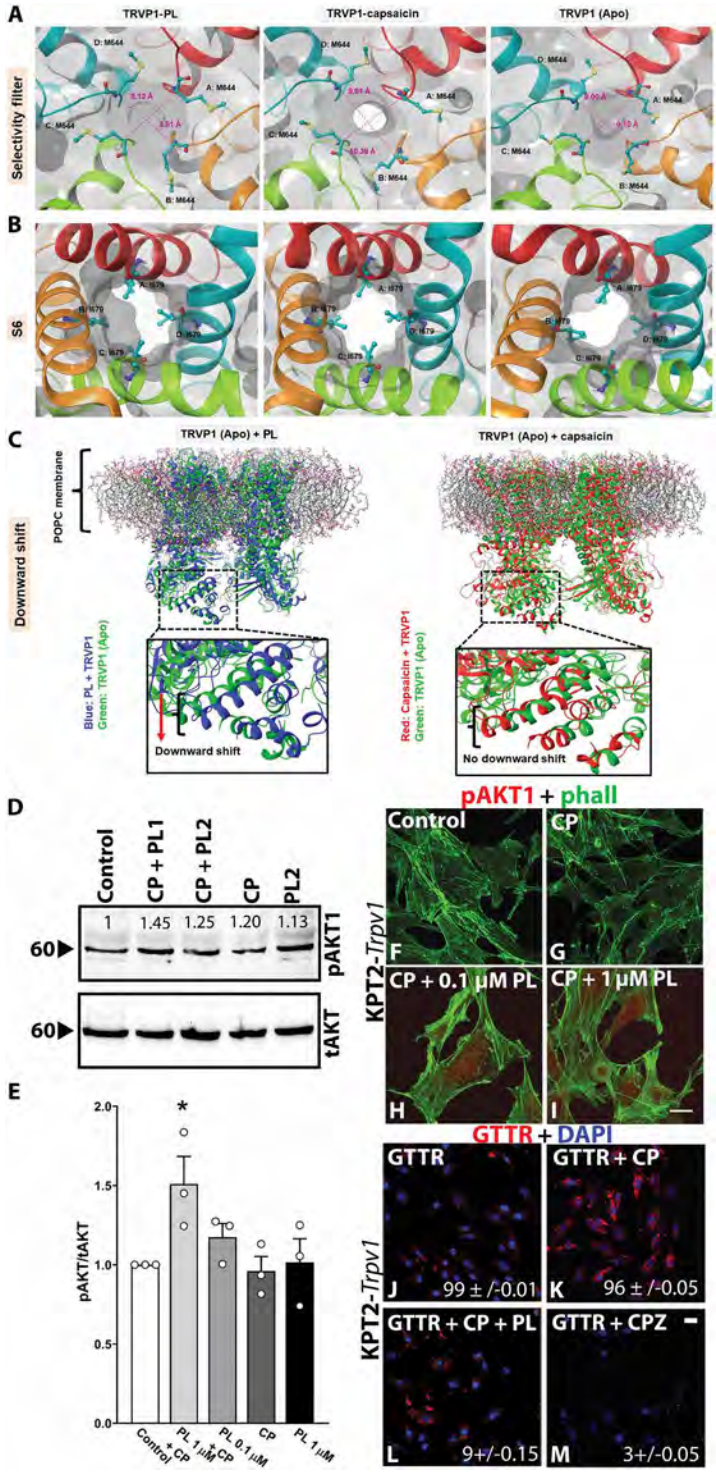

Fig. 8. PL regulates AG uptake through TRPV1 interaction. (**A** and **B**) Structural model depicting the selectivity filter (A) and S6 gate (B) regions of TRPV1 bound to PL (left), CP (center), or unligated (Apo) (right). Images were retrieved from a representative frame of the MD trajectories. TRPV1's chains are presented in different colors. Purple measurements are the distances in angstroms from each carbon alpha from residue M644. (**C**) Structural model of TRPV1 illustrating the receptor upon binding to PL (left) compared with binding to CP (right). (**D**) Representative immunoblot of KPT2 cells stably expressing TRPV1 (KPT2-*Trpv1*), incubated with medium (control), CP + PL (1 μM for CP + PL1 or 0.1 μM for CP + PL2), CP only, or PL only (1 μM; PL2). Numbers indicate pAKT/tAKT ratios for that particular experiment. (**E**) Quantification of pAKT/tAKT ratios from three independent immunoblots. One-way ANOVA followed by Dunnett's posttest for multiple comparisons. *$P < 0.05$ versus CP. (**F** to **I**) Representative images of KPT2-*Trpv1* cells incubated with medium-only (F), CP (G), or CP + PL [0.1 μM for (H) and 1 μM for (I)] and stained for pAKT1 (red) and phalloidin (green). (**J** to **M**) Representative images of KPT2- *Trpv1* cells incubated with GTTR alone (red) (J), GTTR + CP (K), GTTR + CP + PL (1 μM) (L), and GTTR + capsazepine (GTTR + CPZ) (M) counterstained with phalloidin (green). Numbers in (J) to (M) are the percentages of GTTR-positive cells. Scale bars, 20 μm.

binding results in conformational changes across multiple subdomains of TRPV1, leading to a selectivity filter and S6 gate opening (to allow ion conduction) (Fig. 8, A to C) (*40*).

In addition, we analyzed the protein root mean square deviation (RMSD) throughout the entire simulation period (fig. S7D). The RMSD measures the average distance between groups of atoms to determine degrees of conformational changes during MD simulations (*41*). The overall receptor RMSD values for the PL-TRPV1 or Apo complexes were much lower than that for the CP-TRPV1 complex (RMSD: 3.83 ± 0.52, 3.60 ± 0.46, and 5.33 ± 1.19 for PL, Apo, and CP, respectively). This indicates that the CP-TRPV1 complex went through a substantial degree of conformational changes (expected for an ion channel opening) compared with the PL-TRPV1 or Apo complexes. Furthermore, the ligand RMSD (blue and red lines in fig. S7D) indicates that PL is stable in the proposed binding pocket throughout the simulation trajectory (fig. S7D, middle). In conclusion, the results presented in Fig. 8 (A to C) suggest that PL might have a similar interaction with TRPV1 as it does with TRPV2 (*18*), leading to similar structural changes and the closure of the channel.

To assess the functional link between PL, TRPV1, AKT1, and AG uptake, we used an immortalized mouse proximal tubular epithelial cell line (KPT2) stably expressing TRPV1 (KPT2-*Trpv1*) or a retroviral control vector (KPT2-pBabe) (*37*). These lines have already been characterized and used to test the role of TRPV1 during AG uptake (*37*). AKT1 phosphorylation (Fig. 8, D and E) was measured in KPT2-*Trpv1* cells incubated with medium alone, CP (3 μM), PL (1 μM), or CP + PL1 (PL1 = 1 μM or PL2 = 100 nM). Only when the cells were coincubated with CP + PL1, we observed a modest albeit significant ($P < 0.05$) increase in AKT1 phosphorylation. CP, PL-only, and CP + PL2 (100 nM) did not increase pAKT1 quantities. AKT1 phosphorylation was also assessed by immunofluorescence (Fig. 8, F to I). Similarly to the immunoblot results, we observed a positive pAKT1 signal when cells were incubated with CP + PL. No positive signal was detected in nonstimulated cells (control) or cells incubated with CP only (Fig. 8, F and G). Moreover, in the KPT2-pBabe cells (transfected with the empty vector), we observed an increase in pAKT1 (fig. S7E). Last, we performed gentamicin–Texas Red (GTTR) uptake experiments (Fig. 8, J to M) to test whether PL can prevent AG incorporation. Under basal conditions (GTTR control; Fig. 8J), there was minimal incorporation of GTTR by the KPT2-*Trpv1*, whereas coincubation with CP (Fig. 8K) resulted in an increase in GTTR incorporation, confirming previous results (*37*). Conversely, the presence of PL (Fig. 8L) led to a reduction in GTTR uptake. Similar results were obtained when cells were coincubated with the TRPV1 antagonist capsazepine (Fig. 8M). The KPT2-pBabe cells,

which express low levels of TRPV1 (*37*), did not show any detectable GTTR incorporation (fig. S7F).

DISCUSSION

There are no therapies to protect from AGIHL, and although new strategies have been implemented to avoid this societal and economic burden, AGs are still a front-line treatment for severe sepsis (*6*–*5*, *11*). Moreover, given their excellent water solubility, effectiveness, low cost, and stability at room temperature, AGs are the only therapy that is available to treat Gram-negative bacteria infections in developing countries (*1*). Thus, there is an urgent need for the identification of therapies that will prevent patients from losing their hearing when receiving prophylactic or curative AG treatment. Three compounds, ebselen (SPI-1005), ORC-13661, and *N*-acetylcysteine, are currently in clinical trials for the prevention of AGIHL (NCT02819856, NCT05730283, and NCT01271088), and although they showed protection in various animal models, it is still unclear whether the same will apply to humans (*15*, *42*). Moreover, not all patients will respond to the same treatment in a comparable way; race, individual practices and habits, and environmental factors among others will affect the outcome (*43*). Therefore, the search for alternative therapies is still necessary.

An initial screening of a library of small molecules identified PL as a good therapeutic candidate against AGIHL. Further characterization demonstrated that PL has good pharmacological properties (low EC_{50}, high LD_{50}, no DDI, and no interference with AG antibacterial activity). Moreover, when comparing PL with ORC-13661 in the zebrafish ototoxicity model, we found that PL's EC_{50} was lower than that of ORC-13661 (picomolar versus millimolar) and that it did not block MET channel activity (*14*–*15*). Furthermore, PL was protective not only against AG-induced HC loss but also against AG-induced nephrotoxicity.

Given its beneficial features, we moved PL forward and tested it in a more relevant model for AG ototoxicity. For these experiments, we used the B6N(Cg)-Cdh23$^{tm2.1/kjn}$ mouse line that allowed the recording of inner ear function in animals 14 weeks and older without the risk of developing early-onset age-related hearing loss (*29*). This new experimental animal model showed a reduction in sound sensitivity at all of the frequencies tested when treated with kanamycin. Conversely, PL administration reversed this deficit. At lower frequencies, PL was fully protective, whereas at higher frequencies, we only observed partial protection. Overall, in all of the cases, the hearing function of animals cotreated with PL was better than with kanamycin alone, suggesting that PL has therapeutic potential. The comparative analysis between PL, ORC-13661, and ebselen demonstrates that despite the differences in the experimental model, PL has a similar protective effect under current tested conditions as the previously described compounds (*14*–*15*, *42*–*44*).

Analysis of the organ of Corti morphology confirmed the effect of PL treatment, and both HCs and presynaptic ribbons were protected from kanamycin's deleterious side effects. However, despite full morphological protection, the hearing function of these animals was not completely restored. Because the initial analysis was at presynapses, we looked at postsynaptic structures with the hypothesis that the above differences may be a consequence of postsynaptic abnormalities. The complexity, density, and volume of the neuronal fibers innervating the base of the HCs were not affected by any of the treatments, not even by kanamycin alone. Given this, we concluded that additional damage (HC dysfunction, additional synaptic abnormalities, SGN defects, etc.) not detected by our histological assays was present in the kanamycin-only group. This damage, reflected in hearing function, was not prevented by PL treatment, suggesting that additional optimization of PL therapy is needed.

The effect of AGs on the ribbon synapses has been controversial. The bibliography on these matters is limited but suggests that different AGs and administration protocols will result in various synaptic sensitivities. For example, a study performed in CBA/Ca mice receiving tobramycin showed that ribbon synapses are not affected (*44*), whereas another study performed in C57BL6 mice demonstrated that it is only the combination of gentamicin with furosemide that results in ribbon synapse loss (*45*). Conversely, two recent studies have shown a decrease in the presynaptic puncta after the chronic administration of gentamicin (*46*, *47*). Here, we generated a synaptopathy model upon kanamycin treatment that was partially counteracted by PL cotreatment. Thus, given that ORC-13661's and ebselen's therapeutic effects have not been analyzed in the context of synaptopathy (*14*–*15*, *44*), there is no possible comparison, leaving PL as the first and only therapeutic compound that can protect from AG-induced ribbon synapse loss. How relevant this is or how we can extrapolate these results to patients is something that will require additional research, and it is beyond the scope of the present work.

Mechanistically, our results suggest that PI's beneficial effect may be through the down-regulation of TRPV1's expression and the increase in AKT1 activity. The allosteric inhibition of TRPV channels by PL has already been demonstrated (*18*). Here, we also found evidence that suggests that it is not only the activity but also the expression of the channel that may be decreased. We believe that this is happening because of the chronic administration of PL. Thus, the constant binding of PL to TRPV1's allosteric site may have a twofold effect; initially, it blocks activity, but, eventually, it will decrease surface expression. The link between TRPV1 activation and AKT1 inhibition has previously been shown (*35*). In the present work, we found that (i) pAKT1 is reduced during kanamycin treatment (kinome, immunohistochemistry, and immunoblot assays) and (ii) treatment with PL or absence of TRPV1 results in a modest, but significant ($P < 0.05$), activation of AKT1. Last, the link between TRPV1 and AG uptake is suggested by the increase in TRPV1 expression upon AG treatment and the increase in GTTR uptake upon TRPV1 activation [present work and (*32*, *37*, *38*)].

Together, these results suggest that PL-mediated inactivation of TRPV1 can result in a decrease in AG uptake and the beneficial activation of AKT1. At the same time, long-term PL treatment may be decreasing TRPV1 expression, contributing to a reduction in AG uptake. That TRPV1 is involved in AG entry into the inner ear compartment [demonstrated by Steyger's group (*37*) using the TRPV1 knockout mouse] led us to believe that the overall reduction in TRPV1's activity is the main therapeutic effect of PL. Thus, instead of trying to protect the HCs from the AGs that are already in the inner ear compartment, PL might directly block their entrance and, by that, could avoid the problem of long-term AG accumulation in the inner ear. This hypothesis will be tested in future experiments.

Our study has limitations. The evaluation of PL as a therapy against AG ototoxicity was performed in healthy animals; thus, we can only interpret our results within that context. Because AGs are given to treat bacterial infections that can lead, among other things, to an increase in blood-labyrinth barrier (BLB) permeability, additional studies will need to be performed to evaluate the efficacy

and potency of PL under those situations. PL might also have off-target effects that could affect overall therapeutic outcomes. This is something that we will also need to address in future work.

Last, regarding TRPV1 expression in the inner ear compartment, although fluorescent values went back to the control levels in the SV and HC regions of animals cotreated with PL, that was not the case for SGNs. This result is in accordance with the partial recovery of the hearing function observed in animals treated with PL + kanamycin (moderate recoveries of wave I amplitudes and latencies) despite the preservation of OHCs, presynaptic ribbons, and neuronal fibers. Thus, we can speculate that this functional gap between controls and PL-cotreated animals is because PL fails to completely down-regulate TRPV1 in neuronal cell bodies, pointing again to the need to improve PL's chemical structure. In addition and not mutually exclusive, AGs can access the inner ear compartment by other means not regulated by PL (*48*). Although possible, we believe that this is unlikely because it has already been shown that TRPV1 knockout animals are resistant to AGIHL (*37*).

In summary, our findings suggest that PL may be preventing AG ototoxicity by regulating TRPV1 expression and, directly or indirectly, AKT1 activity. This, combined with our molecular docking analysis, provides the basis for future research into the optimization of PL's chemical structure to increase its selectivity, potency, and efficacy. By performing these chemical modifications, we expect to obtain a derivative that will confer full protection against AGIHL. Moreover, future efforts will also be directed toward the characterization of additional PL derivatives for the treatment of other forms of hearing loss.

MATERIALS AND METHODS

Study design

The objective of this study was to test whether PL can preserve hearing function when coadministered during AG treatment. The density of HCs was evaluated with antibody staining and confocal imaging in zebrafish and mice treated with vehicle, AG, PL, or both. ABR and DPOAE functional tests were used to compare hearing phenotypes among mice treated with vehicle, AG, PL, or both. For in vivo studies, each animal (fish/mouse) within a group was considered an independent biological replicate. Animals were randomized into the four groups with an equal number of females and males. Details on the use of cell lines to study PL cytotoxicity and AG uptake can be found in Materials and Methods (the sections "Cell-based, CYP45, and disc diffusion assays" and "KPT2 cell experiments," respectively). For the cell studies, experiments were performed three times, and each experiment was considered an independent biological replicate. The sample size was calculated on the basis of previous experiments performed in our laboratory. Each mouse received an alphanumerical code associated with the treatment to which the person(s) conducting the hearing tests and analysis was blinded. All procedures were performed with the approval of and in accordance with guidelines established by Creighton University Animal Resource Facilities (Institutional Animal Care and Use Committee #1192 and #1197 for experiments on zebrafish and #1108 and #1127 in mice). ARRIVE (Animal Research: Reporting of In Vivo Experiments) guidelines were followed for the generation of this article.

Animal care

Zebrafish and mice were maintained at Creighton University Animal Resource Facilities by standard methods and per the Institutional Animal Care and Use Committee. For PL ototoxicity and FM1-43 uptake experiments, we used 5- to 6-dpf wild-type (TuAB, ZFIN, and OR) and *Tg(brn3c:GFP)* (*28*) zebrafish lines. For proximal tubule integrity assay, 5- to 6-dpf *Tg(lfabp::1/2vdbp-mCherry)* fish was used (*27*). Fish were maintained at 28.5°C in E3 medium (*49*) with a 14-hour light/10-hour dark cycle. The B6N(Cg)-Cdh23$^{tm2.1/kjn}$ mouse line (strain #018399, the Jackson Laboratory) was used for the kanamycin chronic studies and was maintained with a 12-hour light/dark cycle and free access to food and water.

Zebrafish experiments

Ototoxicity studies

Dose-response curves were obtained as previously described (*17*) using various PL concentrations (Cayman Laboratories) (8 μM to 8pM in half steps) in DMSO. After 1 hour, fish were coincubated with PL and 400 μM of kanamycin (VWR, PA) for 5 hours, and HCs were manually counted using a Zeiss AxioSkop2 fluorescence microscope. The inspected neuromasts were part of the cranial system and included the otic, middle, and opercular neuromasts.

FM1-43 uptake

FM1-43 (F35355, Thermo Fisher Scientific, CA) uptake was used as a proxy for MET channel activity. Experiments were performed as previously described (*28*) in the presence of PL at 150 pM (EC_{50}) or 15 nM (×100 EC_{50}). The fluorescence incorporated by the neuromast was quantified using ImageJ and expressed as total fluorescence per neuromast and per HC.

Kidney proximal tubule activity

The *Tg(lfabp::1/2vdbp-mCherry)* zebrafish line was used for these experiments as previously described (*27*). Animals were incubated with kanamycin in the presence of PL (PL3) at 150 pM (EC_{50}), PL2 at 150 nM, and PL1 at 8 μM.

Cell-based, CYP450 and disc diffusion assays

Viability assay

HEI-OC1 cells were grown as previously described (*24*), and the cell viability was assessed with PrestoBlue cell viability reagent (Thermo Fisher Scientific, CA).

Colchicine incubations

HEI-OC1 cells were incubated for 8 hours with 25 μM PL or 10 μM colchicine (C9754, Sigma-Aldrich, MO). Fixed cells were immunostained for α-tubulin.

CYP450 assay

Cytochrome activity in the presence of PL was measured with the Vivid CYP3A5 Green Screening Kit (P2969, Thermo Fisher Scientific, CA). PL was used at 1, 0.2, and 0.04 mM (concentrations in the plateau region of the dose-response curve); 8 and 1.6 nM (concentrations in the upper part of the linear function); and 0.32 nM (concentration in the lower part of the linear dose-response function). Ketoconazole (K1003, Sigma-Aldrich, MO; 10 mM) was used as a positive control for inhibition of CYP450 activity.

Disc diffusion assay

AG efficacy in the presence of PL was performed as previously described (*17*).

Mouse treatment

The paradigm to generate the kanamycin ototoxicity model in mice has been previously described by Koo *et al.* (*36*), with the following modifications: 7- to 8-week-old B6N(Cg)-Cdh23$^{tm2.1/kjn}$ mice received vehicle (corn oil) or PL (40 mg/kg of body weight) in corn oil

intraperitoneally for 17 days. Kanamycin or vehicle (saline solution) administration was given subcutaneously twice a day for 14 days, starting 1 day after the first PL treatment. Weights were monitored, and the PL and kanamycin doses were adjusted every 5 days to reflect the changes in total body weight. Animals were euthanized 4 weeks after the last dose and the posttreatment hearing tests.

Hearing tests

The ABR acquisition and data management were performed using a Tucker-Davis Technologies (TDT; Alachua, FL) RZ6 Multi I/O processor and BioSigRZ software. Stimuli were presented by a TDT MF1 driver placed 10 cm from the left ear of each animal. Tone burst stimuli of a 5-ms duration at half-octave frequency intervals from 4.0 to 64 kHz were presented at 19 per second. At each frequency, an intensity series was presented from 20- to 100-dB SPL (decibel sound pressure level) in 5-dB steps. After the hearing baseline measurements, animals were allowed to recover from anesthesia for 1 to 3 days before the initiation of the treatment. Only one animal (female) was excluded during the hearing test experiments because of an abnormal baseline ABR.

For DPOAEs, the primary tones f1 and f2 were generated and shaped using the TDT's hardware. DPOAEs were recorded in the form of level/frequency functions; f2/f1 was fixed at 1.2, with the level of the f2 (L2) 10 dB lower than the f1 level (L1). Signal was collected by an ER10B+ (Etymotic) microphone.

Endocochlear potentials

Endocochlear potentials were measured at least 24 hours after the last hearing test, and the inner ears were immediately isolated and processed for immunohistochemistry. For the endocochlear potentials, a round window approach was taken from the cochlear basal turn as previously described (*50*).

PL detection in the inner ear compartment

Animals received PL (40 mg/kg) or corn oil intraperitoneally. After 2 hours, the inner ears were microdissected and homogenized, and PL was extracted and processed for liquid chromatography with tandem mass spectrometry as previously described (*22*).

Kinome analyses

Identification of significant differential AKT family kinase activity

Twenty-three AKT kinase family putative target peptides were identified by the kinome random sampling analyzer package (*34*). Log_2 fold changes (FCs) in peptide activity were calculated by comparing kanamycin, PL, or kanamycin + PL with vehicle control. For each peptide, an average of triplicates was used per condition. The technical triplicates of each condition were highly reproducible (fig. S8). Two-way analysis of variance (ANOVA) was used to identify significant differences (***$P < 0.001$).

Methods omnibus for the PamGene kinome array

The STK PamGene12 chips have 144 reporter peptides (*51*). The sample was added to one of the four-well peptide chips, and phosphorylation was detected in real time with fluorescent antibodies. Fluorescent intensity was used as a proxy for the extent of reporter peptide phosphorylation (fig. S8A), and altered kinase activity could be directly measured. Of the about 500 kinases in the human genome (*52*), 65% can be mapped to the STK chip with a detection sensitivity in the picogram range.

Kinome array protocols

Samples were prepared according to PamGene Corp (https://pamgene.com/ps12/). Peptide phosphorylation was monitored during the incubation. The primary output is images that are then preprocessed to quantify the activity at each peptide concentration using the PamGene's BioNavigator software (https://pamgene.com/wp-content/uploads/2020/09/BioNavigator-User-Manual-vs2.3-2020.pdf), and inactive peptides (raw signal ≤ 5) were removed from the analysis. The dynamic range of the raw signal intensities was typically 0 to 3000. Linear regression slope of the signal intensity as a function of exposure time was used to represent the peptide phosphorylation intensity for downstream comparative analyses. The signal ratio between case and control samples was used to calculate FC values. Peptides with an FC of at least 15% (FC > 1.15 or FC < 0.85) were considered differentially phosphorylated. This threshold was chosen on the basis of previous reports that suggest that minor changes in kinase activity are sufficient to trigger biologically relevant changes (*53*). Peptides that had a very low signal or an $R^2 < 0.90$ were excluded from subsequent analyses.

Peptides spotted on the array can be phosphorylated by more than one kinase. Three different software packages were deployed for the assignment of upstream kinases:

1) Upstream kinase analysis package (PamGene Corps'-Hertengobosch, Netherlands) relies on a curated database of kinase-substrate interactions created by the PamGene Corp.

2) Kinome random sampling analyzer relies on a curated database of upstream kinases that were identified using GPS 3.0 and Kinexus Phosphine (*53*).

3) Integration of upstream kinase assignments across packages. All of the tools above use different methods to assign upstream kinases. To identify consensus upstream kinases across datasets, we used the software Creedenzymatic (*53*) that takes in the results from the analyses and generates a consensus figure with kinases deconvolved and ranked on the basis of their presence in the results.

Immunoblot assay

For the immunoblot studies, organs of Corti were collected from the different treatments, processed, and used to run Western blots for AKT1 and ERK proteins as previously described (*17*).

Immunohistochemistry and confocal microscopy

Fish were fixed and immunostained for the HC marker, otoferlin (HC count), or directly washed and mounted (FM1-43 uptake) (*17*). The inner ears were microdissected and processed as previously described (*54*). Samples were immunostained for myosin-7A, Ctbp2, Sox2, neurofilament H, pAKT1, and TRPV1. Images were captured with a Zeiss LSM 700 at room temperature with automatically set sectioning and processed with ZEN black edition software. *z*-stacks are presented as flat *z*-projections. Total fluorescence intensities were calculated using ImageJ (US National Institutes of Health). The neuronal fiber analysis was performed using the filament tracing tool from Imaris. The OHCs were manually counted. Ctbp2 puncta were quantified using the Analyzed Particles tool in ImageJ after thresholding. Adjusted parameters were as follows: pixel size = 0.2 to infinity, and circularity = 0.50 to 1.00. Results were visually confirmed for any missing or additional puncta. Final figures were assembled using Adobe Photoshop.

Molecular docking and MD simulations

Receptor and ligand preparation was performed using the protein wizard tool from Maestro (*55*). To place PL in the same allosteric binding pocket presented in the crystal structure of TRVP2 [Protein Data Bank (PDB) code: 6WKN], we overlaid this protein with the TRPV1 (PDB code: 7LPE) homolog using the MatchMaker structure comparison tool (*56*). Then, we selected the corresponding binding residues in TRPV1 to identify the binding pocket (fig. S7, A and B). Next, using Autodock Vina (*57*–*58*), PL was docked, and the most stable conformation generated (best binding affinity) was selected to be analyzed by MD simulation. Autodock Vina uses a fixed target/flexible ligand approach, with a generic algorithm for the search step, and a hybrid function based on empirical data combined with a knowledge-based function (*55*). In the molecular docking step, the center of the selected residues was used as the reference to create the cubic virtual space (grid) needed to perform the search. The grid center was set at 34.5 Å (*x*), 32.4 Å (*y*), and 25.1 Å (*z*). This positioning and volume were adequate to cover the binding site. The exhaustiveness parameter (which indicates the time spent searching for a global minimum in each docking calculation) was set to 60. This way, the chances of obtaining both a suitable molecular docking methodology and adequate and reliable best poses for the purpose of the study are increased.

MD simulations were used to analyze the dynamic behavior of the TRPV1 receptor bound to PL, agonist control (CP, PDB code: 7LPE), or Apo (*55*). All simulations were conducted using rat TRPV1 (PDB code: 7LPE). A phosphatidylcholine (POPC) membrane was placed on the receptor according to the orientation calculated using the online Orientation of Proteins in Membranes Server (*59*). Each receptor-ligand complex or Apo was placed in an orthorhombic box with periodic boundaries. The box was filled with TIP_3P (transferable intermolecular potential with three points) water and Na^+ or Cl^- ions, which were added to neutralize the system. In addition, 0.15 M NaCl was added to mimic a physiological ion concentration. Next, the system was relaxed using positionally restricted dynamics following the standard Desmond protocol (*60*). All simulations were performed on an NPT (constant particle number, pressure, and temperature) ensemble at a temperature of 300 K and a pressure of 1013 bar. The MD simulation time was set to 250 ns for all complexes. The energy (kcal/mol) was recorded at each 1.2-ps interval. All simulations were performed with a Desmond graphics processing unit using the OPLS3e force field through the Holland Computer Center (*60*). The OPLS3e force field is based on optimized potentials for liquid simulations (OPLS) (*61*). A model of the final set of simulated systems is shown in fig. S7C. The post-MD analyses were performed using the simulation interaction diagram tool, and images were created using the Maestro graphical interface (*55*).

KPT2 cell experiments

Experiments were performed as previously described by Jiang *et al.* (*37*). Briefly, for AKT activity assessment, KPT2 cells (*37*) were incubated for 5 min with Dulbecco's modified Eagle's medium + 1.8 mM $CaCl_2$ and CP (3 μM), CP + PL (1 or 0.1 μM), or PL-only (1 μM), followed by immunoblot or immunocytochemistry processing. For GTTR uptake experiments, KPT2 cells were incubated for 3 min with Dulbecco's modified Eagle's medium + 1.8 mM $CaCl_2$ + GTTR (5 μg/ml) (*37*) alone or CP (S1990, Selleck Chemicals, TX; 3 μM), capsazepine (S8137, Selleck Chemicals, TX; 15 μM), or CP + PL (1 μM) followed by confocal processing.

Antibodies and special reagents

Antibodies used were anti-otoferlin [HCS-1, DSHB (Developmental Studies Hybridoma Bank), IA; 1:100], anti–myosin-7A (25-6790, Proteus Biosciences, MA; 1:400), anti-Ctbp2 (612044, BD Biosciences, NJ, RRID: AB_399431; 1:200), anti–neurofilament H (AB5539, Sigma-Aldrich, MO; 1:1000), anti–α-tubulin (T8203, Sigma-Aldrich, MO; 1:200), anti-TRPV1 (A8564, ABclonal, MA; 1:200), anti–AKT1-S473 (9271), anti-panAKT (4691), anti–ERK1/2 T202/Y204 (9101) and anti-ERK1/2 (9102) (Cell Signaling Technology, MA; 1:750), and anti-Sox2 (14-9811-82, ThermoFisher, CA, RRID: AB_11219471; 1:300). PL was obtained from Cayman Chemicals (11006), kanamycin for zebrafish from VWR (75856-686), and kanamycin for mice from Sigma-Aldrich (K0254).

Statistical analysis

Brown-Forsythe and Welch ANOVA followed by Dunnett's T3 posttest for multiple comparisons and one-way or two-way ANOVA followed by Dunnett's posttest for multiple comparisons were performed using GraphPad v10.0.2. Results are expressed as means ± SEM. Five or six fish were used per experiment, and at least three rostral neuromasts were inspected. Mouse numbers are included in the figures (between brackets) or represented as circles.

Supplementary Materials

This PDF file includes:
Figs. S1 to S8

Other Supplementary Material for this manuscript includes the following:
Data files S1 and S2
MDAR Reproducibility Checklist

REFERENCES AND NOTES

1. World Health Organization, "World report on hearing," (WHO, 2021); www.who.int/publications-detail-redirect/world-report-on-hearing.
2. X. Fu, P. Wan, P. Li, J. Wang, S. Guo, Y. Zhang, Y. An, C. Ye, Z. Liu, J. Gao, J. Yang, J. Fan, R. Chai, Mechanism and prevention of ototoxicity-induced by aminoglycosides. *Front. Cell. Neurosci.* **15**, 692762 (2021).
3. US Food and Drug Administration, "FDA approves sodium thiosulfate to reduce the risk of ototoxicity associated with cisplatin in pediatric patients with localized, non-metastatic solid tumors," (FDA, 2024); https://www.fda.gov/drugs/resources-information-approved-drugs/fda-approves-sodium-thiosulfate-reduce-risk-ototoxicity-associated-cisplatin-pediatric-patients.
4. J. Kim, S. Hemachandran, A. Cheng, A. Ricci, Identifying targets to prevent aminoglycoside ototoxicity. *Mol. Cell. Neurosci.* **120**, 103722 (2022).
5. Cystic Fibrosis Foundation, "About cystic fibrosis"; www.cff.org/intro-cf/about-cystic-fibrosis.
6. V. Arora, D. Strunk, S. Furqan, L. Schweig, C. Lefaiver, J. George, P. Prazad, Optimizing antibiotic use for early onset sepsis: A tertiary NICU experience. *J. Neonatal Perinatal Med.* **12**, 301–312 (2019).
7. J. McDermott, A. Mahaveer, R. James, N. Booth, M. Turner, K. Harvey, G. Miele, G. Beaman, D. Stoddard, K. Tricker, R. Corry, J. Garlick, S. Ainsworth, T. Beevers, I. Bruce, R. Body, F. Ulph, R. MacLeod, P. Roberts, P. Wilson, W. Newman, Rapid point-of-care genotyping to avoid aminoglycoside-induced-ototoxicity in neonatal intensive care. *JAMA Pediatr.* **176**, 486–492 (2022).
8. B. Meatherall, D. Gregson, T. Ross, J. Pitout, K. Laupland, Incidence, risk factors, and outcomes of *Klebsiella pneumoniae* bacteremia. *Am. J. Med.* **122**, 866–873 (2009).
9. K. Wargo, J. Edwards, Aminoglycoside-induced nephrotoxicity. *J. Pharm. Pract.* **27**, 573–577 (2014).
10. L. Dillard, R. Martinez, L. Perez, A. Fullerton, S. Chadha, C. McMahon, Prevalence of aminoglycoside-induced hearing loss in drug-resistant tuberculosis patients: A systematic review. *J. Infect.* **83**, 27–36 (2021).
11. D. Sharma, B. Kumar, M. Lata, B. Joshi, K. Venkatesan, S. Shukla, D. Bisht, Comparative proteomic analysis of aminoglycosides resistant and susceptible *Mycobacterium tuberculosis* clinical isolates for exploring potential drug targets. *PLOS ONE* **10**, e0139414 (2015).
12. D. Fox, M. Cooper, C. Speil, M. Roberts, S. Yanik, R. Meech, T. Hargrove, S. Verhulst, L. Rybak, K. Campbell, D-Methionine reduces tobramycin-induced-ototoxicity without antimicrobial interference in animal models. *J. Cyst. Fibros.* **15**, 518–530 (2016).

13. A. Salt, J. Hartsock, F. Piu, J. Hou, Dexamethasone and dexamethasone phosphate entry into perilymph compared for middle ear applications in guinea pigs. *Audiol. Neurootol.* **23**, 245–257 (2018).
14. S. Chowdhury, K. Owens, R. Herr, Q. Jiang, X. Chen, G. Johnson, V. Groppi, D. Raible, E. Rubel, J. Simon, Phenotypic optimization of urea-thiophene carboxamides to yield potent, well tolerated, and orally active protective agents against aminoglycoside-induced hearing loss. *J. Med. Chem.* **61**, 84–97 (2018).
15. S. Kitcher, N. Kirkwood, E. Camci, P. Wu, R. Gibson, V. Redila, J. Simon, E. Rubel, D. Raible, G. Richardson, C. Kros, ORC-13661 protects sensory hair cells from aminoglycoside and cisplatin ototoxicity. *JCI Insight* **4**, 126764 (2019).
16. I. Kocyigit, "Phase 3 study of protective effect of *N*-acetylcysteine against ototoxicity," ClinicalTrials.gov identifier: NCT01271088 (2011); https://clinicaltrials.gov/study/NCT01271088.
17. M. Zallocchi, S. Hati, Z. Xu, W. Hausman, H. Liu, D. He, J. Zuo, Characterization of quinoxaline derivatives for protection against iatrogenically-induced hearing loss. *JCI Insight* **6**, 141561 (2021).
18. J. Conde, R. Pumroy, C. Baker, T. Rodrigues, A. Guerreiro, B. Sousa, M. C. Marques, B. P. de Almeida, S. Lee, E. Leites, D. Picard, A. Samanta, S. Vaz, F. Sieglitz, M. Langini, M. Remke, R. Roque, T. Weiss, M. Weller, Y. Liu, S. Han, F. Corzana, V. Morais, C. Faria, T. Carvalho, P. Filippakopoulos, B. Snijder, N. Barbosa-Morais, V. Moiseenkova-Bell, G. Bernardes, Allosteric antagonist modulation of TRPV2 by piperlongumine impairs glioblastoma progression. *ACS Cent. Sci.* **7**, 868–881 (2021).
19. K. Lewis, U. Bharadwaj, T. Eckols, M. Kolosov, M. Kasembeli, C. Fridley, R. Siller, D. Tweardy, Small-molecule targeting of signal transducer and activator of transcription (STAT) 3 to treat non-small cell lung cancer. *Lung Cancer* **90**, 182–190 (2015).
20. Q. Zhang, W. Chen, X. Lv, Q. Weng, M. Chen, R. Cui, G. Liang, J. Ji, Piperlongumine, a novel TrxR1 inhibitor, induces apoptosis in hepatocellular carcinoma cells by ROS-mediated ER stress. *Front. Pharmacol.* **10**, 1180 (2019).
21. E. Mgbeahuruike, M. Stålnacke, H. Vuorela, Y. Holm, Antimicrobial and synergistic effects of commercial piperine and piperlongumine in combination with conventional antimicrobials. *Antibiotics* **8**, E55 (2019).
22. J. Liu, W. Liu, Y. Lu, H. Tian, C. Duan, L. Lu, G. Gao, X. Wu, X. Wang, H. Yang, Piperlongumine restores the balance of autophagy and apoptosis by increasing BCL2 phosphorylation in rotenone-induced parkinson disease models. *Autophagy* **14**, 845–861 (2018).
23. S. Kumar, N. Agnihotri, Piperlongumine, a piper alkaloid targets Ras/PI3K/Akt/mTOR signaling axis to inhibit tumor cell growth and proliferation in DMH/DSS induced experimental colon cancer. *Biomed. Pharmacother.* **109**, 1462–1477 (2019).
24. G. Kalinec, P. Thein, C. Park, F. Kalinec, HEI-OC1 cells as a model for investigating drug cytotoxicity. *Hear. Res.* **335**, 105–117 (2016).
25. D. Hoti, O. Rustem, Avermectin B1a shows potential anti-proliferative and anticancer effects in HCT-116 cells via enhancing the stability of microtubules. *Curr. Iss. Mol. Bio.* **45**, 6272–6282 (2023).
26. M. Mingeot-Leclercq, P. Tulkens, Aminoglycosides: Nephrotoxicity. *Antimicrob. Agents Chemother.* **43**, 1003–1012 (1999).
27. Z. Chen, A. Luciani, J. Mateos, G. Barmettler, R. Giles, S. Neuhauss, O. Devuyst, Transgenic zebrafish modeling low-molecular-weight proteinuria and lysosomal storage diseases. *Kidney Int.* **97**, 1150–1163 (2020).
28. O. Ogun, M. Zallocchi, Clarin-1 acts as a modulator of mechanotransduction activity and presynaptic ribbon assembly. *J. Cell Biol.* **207**, 375–391 (2014).
29. K. Kane, C. Longo-Guess, L. Gagnon, D. Ding, R. Salvi, K. Johnson, Genetic background effects on age-related-hearing-loss associated with Cdh23 variants in mice. *Hear. Res.* **283**, 80–88 (2012).
30. C. Dai, D. Mangiardi, D. Cotanche, P. Steyger, Uptake of fluorescent gentamicin by vertebrate sensory cells in vivo. *Hear. Res.* **213**, 64–78 (2006).
31. A. Garinis, C. Cross, P. Srikanth, K. Carroll, M. Feeney, D. Keefe, L. Hunter, D. Putterman, D. Cohen, J. Gold, P. Steyger, The cumulative effects of intravenous antibiotic treatments on hearing in patients with cystic fibrosis. *J. Cys. Fib.* **16**, 401–409 (2017).
32. K. Hirose, S.-Z. Li, K. Ohlemiller, R. Ransohoff, Systemic lipopolysaccharide induces cochlear inflammation and exacerbates the synergistic ototoxicity of kanamycin and furosemide. *J. Assoc. Res. Otolaryngol.* **15**, 555–570 (2014).
33. M. Liberman, S. Kujawa, Cochlear synaptopathy in acquired sensorineural hearing loss: Manifestations and mechanisms. *Hear. Res.* **349**, 138–147 (2017).
34. K. Alganem, A. Hamoud, J. Creeden, N. Henkel, A. Imami, A. Joyce, V. Ryan, J. Rethman, R. Shukla, S. O'Donovan, J. Meller, R. McCullumsmith, The active kinome: The modern view of how active protein kinase networks fit in biological research. *Curr. Opin. Pharmacol.* **62**, 117–129 (2022).
35. X. Wang, Y. Bian, C. Wong, J. Lu, S. Lee, TRPV1 modulator ameliorates alzheimer-like amyloid-β neuropathology via Akt/Gsk3β-mediated Nrf2 activation in the Neuro-2a/APP cell model. *Oxid. Med. Cell Longev.* **2022**, e1544244 (2022).
36. J. Koo, L. Quintanilla-Dieck, M. Jiang, J. Liu, Z. Urdang, J. Allensworth, C. Cross, H. Li, P. Steyger, Endotoxemia-mediated inflammation potentiates aminoglycoside-induced ototoxicity. *Sci. Transl. Med.* **7**, 298ra118 (2015).
37. M. Jiang, H. Li, A. Johnson, T. Karasawa, Y. Zhang, W. Meier, F. Taghizadeh, A. Kachelmeier, P. Steyger, Inflammation up-regulates cochlear expression of TRPV1 to potentiate drug-induced hearing loss. *Sci. Adv.* **5**, eaaw1836 (2019).
38. D. Mukherjea, S. Jajoo, K. Sheehan, T. Kaur, S. Sheth, J. Bunch, C. Perro, L. P. Rybak, V. Ramkumar, NOX3 NADPH oxidase couples transient receptor potential vanilloid 1 to signal transducer and activator of transcription 1-mediated inflammation and hearing loss. *Antioxid. Redox Signal.* **14**, 999–1010 (2011).
39. A. Perálvarez-Marín, P. Doñate-Macian, R. Gaudet, What do we know about the transient receptor potential vanilloid 2 (TRPV2) ion channel? *FEBS J.* **280**, 5471–5487 (2013).
40. D. Kwon, F. Zhang, Y. Suo, J. Bouvette, M. Borgnia, S. Lee, Heat-dependent opening of TRPV1 in the presence of capsaicin. *Nat. Struct. Mol. Biol.* **28**, 554–563 (2021).
41. W. Schreiner, R. Karch, B. Knapp, N. Ilieva, Relaxation estimation of RMSD in molecular dynamics immunosimulations. *Comput. Math. Methods Med.* **2012**, 1–9 (2012).
42. Clinicaltrials.gov search results for "hearing loss," https://clinicaltrials.gov/search?cond=hearing%20loss.
43. L. S. Gonzalez III, J. Spencer, Aminoglycosides: A practical review. *Am. Fam. Physician* **58**, 1811–1820 (1998).
44. R. Gu, R. Longenecker, J. Homan, J. Kil, Ebselen attenuates tobramycin-induced-ototoxicity in mice. *J. Cyst. Fibros.* **20**, 271–277 (2021).
45. L. Sargsyan, A. Hetrick, J. Gonzalez, M. Leek, G. Martin, H. Li, Effects of combined gentamicin and furosemide treatment on cochlear ribbon synapses. *Neurotoxicology* **84**, 73–83 (2021).
46. L. Gen, Y. Goo, H. Wu, T. Zhoo, Gentamicin administration leads to synaptic dysfunction in inner hair cells. *Toxicology Lett.* **391**, 86–99 (2024).
47. K. Liu, D. Che, W. Guo, N. Yu, X. Wang, Z. Hou, W. Yang, S. Yang, Spontaneous and partial repair of ribbon synapse in cochlear inner hair cells after ototoxic withdrawal. *Mol. Neurobiol.* **52**, 1680–1689 (2015).
48. J. Kim, J. A. J. Ricci, In vivo real-time imaging reveals megalin as the aminoglycoside gentamicin transporter into cochlea whose inhibition is otoprotective. *Proc. Natl. Acad. Sci. U.S.A.* **119**, e2117946119 (2022).
49. M. Westerfield, *The Zebrafish Book: A Guide for the Laboratory Use of Zebrafish Danio* (Brachydanio) rerio* (University of Oregon Press, 2007); https://zfin.org/zf_info/zfbook/zfbk.html.
50. Y. Li, H. Liu, X. Zhao, D. He, Endolymphatic potential measured from developing and adult mouse inner ear. *Front. Cell. Neurosci.* **14**, 584928 (2020).
51. R. Hilhorst, L. Houkes, A. van den Berg, R. Ruijtenbeek, Peptide microarrays for detailed, high-throughput substrate identification, kinetic characterization, and inhibition studies on protein kinase A. *Anal. Biochem.* **387**, 150–161 (2009).
52. G. Manning, Genomic overview of protein kinases, in *WormBook*, the *C. elegans* Research Community, Eds. (WormBook, 2005) pp. 1–19; http://www.wormbook.org/chapters/www_genomicoverviewkinases/genomicoverviewkinases.html.
53. J. Creeden, Z. Kipp, M. Xu, R. Flight, H. Moseley, G. Martinez, W. Lee, K. Alganem, A. Imami, M. McMullen, S. Roychowdhury, A. Nawabi, J. Hipp, S. Softic, S. Weinman, R. McCullumsmith, L. Nagy, T. Hinds, Hepatic kinome atlas: An in-depth identification of kinase pathways in liver fibrosis of humans and rodents. *Hepatology* **76**, 1376–1388 (2022).
54. M. Zallocchi, D. Meehan, D. Delimont, J. Rutledge, M. Gratton, J. Flannery, D. Cosgrove, Role for a novel usher protein complex in hair cell synaptic maturation. *PLOS ONE* **7**, e30573 (2012).
55. Life science–Schrödinger, www.schrodinger.com/life-science/.
56. E. Pettersen, T. Goddard, C. Huang, G. Couch, D. Greenblatt, E. Meng, T. Ferrin, UCSF chimera—A visualization system for exploratory research and analysis. *J. Comput. Chem.* **2**, 1605–1612 (2004).
57. O. Trott, A. Olson, AutoDock vina: Improving the speed and accuracy of docking with a new scoring function, efficient optimization, and multithreading. *J. Comput. Chem.* **31**, 455–461 (2010).
58. S. Dallakyan, A. Olson, Small-molecule library screening by docking with PyRx. *Methods Mol. Biol.* **1263**, 243–250 (2015).
59. M. A. Lomize, I. D. Pogozheva, H. Joo, H. I. Mosberg, A. L. Lomize, OPM database and PPM web server: Resources for positioning of proteins in membranes. *Nucleic Acids Res.* **40**, D370–D376 (2012).
60. Holland Computing Center, https://hcc.unl.edu/.
61. K. Roos, C. Wu, W. Damm, M. Reboul, J. Stevenson, C. Lu, M. Dahlgren, S. Mondal, W. Chen, L. Wang, R. Abel, R. Friesner, E. Harder, OPLS3e: Extending force field coverage for drug-like small molecules. *J. Chem. Theory Comput.* **15**, 1863–1874 (2019).

Acknowledgments: This research was conducted in the CU AVT Core (GM103427/GM139762) and the UNMC Advanced Microscopy Core (RRID:SCR_022467/P20GM103427/P30GM106397/P30CA036727). We thank H. Jensen-Smith and R. Vielman-Quevedo for technical assistance and I. Fedorchuk for the artwork. We thank P. Steyger for the KPT2 cell lines, the Animal Resource Facility staff for mouse husbandry, and X. Liu for zebrafish husbandry. **Funding:** This work was supported by 1R43DC019065-01 to M.Z., CU startup-fund 240257-822525 to M.Z., and the state of Nebraska LB692 to J.Z. **Author contributions:** M.Z., S.V., and J.F.

conceptualized the study. M.Z., A.S.I., A.-R.A.H., R.M., M.C.-S., and L.J.D.C. curated the data. Formal analysis was performed by M.Z., A.S.I., A.-R.A.H., and L.J.D.C. The investigation was performed by M.Z., S.V., L.B., K.E.B., D.S., H.L., D.Z.Z.H., A.S.I., A.-R.A.H., and L.J.D.C. Methodology was developed by M.Z., J.F., S.V., Z.C., O.D., R.M., D.Z.Z.H, and M.C.-S. M.Z., M.C.S, and L.J.D.C wrote the paper. M.Z. and J.Z. provided funding. **Competing interests:** J.Z. is a cofounder of Ting Therapeutics LLC. J.Z. and M.Z. have filed a provisional patent on PL ("Composition and methods for the prevention of aminoglycoside toxicity," 18/031,99) for hearing loss therapy. The other authors declare that they have no competing interests. **Data and materials availability:** All data needed to evaluate the conclusions in the paper are present in the paper and/or the Supplementary Materials. The *Tg(lfabp::1/2vdbp-mCherry)* zebrafish line was obtained from the laboratory of O.D. at the University of Zürich through a material transfer agreement. All other fish and cell lines are available from the corresponding author, M.Z., under a material transfer agreement with Creighton University.

Submitted 1 December 2023
Resubmitted 17 March 2024
Accepted 28 June 2024
Published 7 August 2024
10.1126/scitranslmed.adn2140